Stress effect on Raman spectra of Ce-doped $BaTiO_3$ films

2000 J. Phys.: Condens. Matter 12 7013

(http://iopscience.iop.org/0953-8984/12/31/303)

J. Phys.: Condens. Matter **12** (2000) 7013–7023. Printed in the UK PII: S0953-8984(00)13194-7

Stress effect on Raman spectra of Ce-doped $BaTiO_3$ films

M S Chen†, Z X Shen†§, S H Tang†, W S Shi‡, D F Cui‡ and Z H Chen‡

† Department of Physics, National University of Singapore, Lower Kent Ridge Road, Singapore 119260

‡ Laboratory of Optical Physics, Institute of Physics and Center for Condensed Matter Physics, Chinese Academy of Sciences, Beijing 100080, China

E-mail: physzx@nus.edu.sg

Received 12 April 2000

Abstract. Ce-doped $BaTiO_3$ (BTO:Ce) thin films prepared on MgO (100) substrates by pulsed laser deposition (PLD) at oxygen pressure of 1.2×10^{-3} and 17 Pa have been studied by micro-Raman spectroscopy, x-ray diffraction (XRD) and atomic force microscopy (AFM). The film deposited at lower oxygen pressure has a larger lattice parameter in the direction normal to the substrate surface, and the film has smaller grains and a smoother surface. The polarized Raman peaks of both as-deposited films show blue shifts and linewidth broadening in comparison to those of the $BaTiO_3$ single crystal. The blue shifts are attributed to tensile stresses in the films. Our results indicate that the grain size increases and the tensile stress relaxes with annealing. We have shown that quantum confinement and oxygen vacancies are not the dominant factors for the observed Raman spectral changes.

1. Introduction

Ferroelectrics have long been studied in connection with numerous functional devices owing to the various properties such as ferroelectricity, piezoelectricity and pyroelectricity. In the last decade, ferroelectric films attracted great attention. On one hand, their ferroelectric, dielectric and piezoelectric properties were promising for their potential applications in various fields of microelectronics and optoelectronics, such as infrared sensors and detectors, high-density dynamic random access memories (DRAMs), non-volatile ferroelectric random access memories (FRAMs) and non-linear optoelectronic devices. On the other hand, the physical properties of ferroelectric thin films were found to be substantially different from those of the bulk ferroelectrics [1–3]. The following need to be considered in the study of thin films, (1) the film–substrate interaction at the interface which primarily induces stress in the films, (2) the grain size effect of the films which are related to both quantum confinement and stress, (3) defects, particularly oxygen defects in our case, which are mainly controlled by growth parameters but can also be varied by post-growth treatment such as annealing in oxygen or vacuum, (4) other factors, e.g. the orientation of the grains.

Stress has always been one of the major interests in the study of ferroelectric thin films. Film stresses, including thermal stress due to the thermal expansion coefficient difference between film and substrate, intrinsic stress determined by growth parameters and extrinsic stress caused by structural changes, can significantly change mechanical, dielectric and optical properties and influence the nature of phase transitions [4]. For $BaTiO_3$ thin films, compressive

§ To whom correspondence should be addressed. Fax: 65-7776126.

0953-8984/00/317013+11$30.00

stress can decrease the optical band gap while the reverse is true for tensile stress [4, 5]. The effects of stress on the Curie point of the $BaTiO_3$ and $PbTiO_3$ thin films were studied both experimentally and theoretically [6–11]. It has also been shown that the two-dimensional stress in the thin films can have a strong influence on the dielectric constant [12] and strain relaxation is strongly related to domain formation in ferroelectric thin films [8, 13–16]. Grain size has a major influence on crystal structure and properties of ferroelectric materials [17–25]. For ultra-fine $BaTiO_3$ and $PbTiO_3$ particles, both the Curie temperature and dielectric constant decrease with decrease in grain size [20–24]. Moreover, there is a strong relationship between grain size and stress [5, 20, 23–25].

$BaTiO_3$ has been successfully doped with Cerium to form Ce-doped $BaTiO_3$ (BTO:Ce) single crystals with superior photorefractive properties and better ferroelectric and electro-optic properties [26, 27]. BTO:Ce thin films prepared by PLD showed a larger linear electro-optic coefficient and obvious hysteresis in the quadratic electro-optic coefficient [28]. In this paper, BTO:Ce films has been investigated using Raman spectroscopy in combination with x-ray diffraction (XRD) and atomic force microscopy (AFM). Raman spectroscopy has been demonstrated as a powerful tool to study stress and size effects in ferroelectric thin films [5–7, 25, 29–31].

2. Experimental details

The BTO:Ce thin films used in this study were grown on MgO(100) substrates by the pulsed laser deposition (PLD) technique using a XeCl excimer laser. Details of the growth were similar to those described previously [32], except that a Ce-doped single crystal BTO target was used in our case. The growth parameters are given in table 1. Sample (1) grown at 17 Pa oxygen pressure has larger grains and is almost O defect free, while sample (2) grown at 1.2×10^{-3} Pa has much smaller grains and contains a substantial number of O vacancies (detailed discussions are given in latter sections). The grains in both films are preferentially oriented with their *c*-axis perpendicular to the substrate surface, i.e., *c*-oriented domains. The Ce concentration is $\sim$ 50 ppm and the thickness of the films is between 50–100 nm with sample (1) thinner than sample (2). We have carried out post annealing between 600–750 °C in either air or vacuum, in order to investigate the size and stress effects.

Table 1. Growth parameters of BTO:Ce thin films deposited by pulsed laser deposition.

Sample	(1)	(2)
Substrate	MgO (100)	MgO (100)
Laser energy	260 mJ	260 mJ
Laser repetition rate	10 Hz	4 Hz
Substrate temperature	$\sim$ 600 °C	$\sim$ 600 °C
Oxygen pressure	17 Pa	1.2×10^{-3} Pa

All micro-Raman spectra were measured at room temperature in the backscattering geometry using a Spex 1702/04 single-grating Raman spectrometer with an Olympus microscope attachment and equipped with a liquid-nitrogen-cooled CCD detector. The laser excitation line was rejected using a pair of super notch filters with a cut-off wavenumber of 150 cm^{-1}. The 488 nm line of an argon-ion laser was used as the excitation source and the instrumental resolution was $\sim$ 0.7 cm^{-1}. Typical Raman spectra were recorded with 10 mW laser power using a 100× microscope objective with NA 0.95. Two scattering geometries, parallel and cross polarizations were used to obtain the polarized Raman spectra. The lattice

parameters of the films were analysed by XRD, and AFM was used to observe the surface topography and grain size of the films.

3. XRD, AFM results and discussion

Figure 1 displays the XRD patterns of the as-deposited BTO:Ce films, where all the observed peaks can be indexed to (00l) diffraction. Table 2 lists the film lattice parameters normal to the substrate surface, which were calculated from the 2θ-values of the XRD patterns for the as-deposited and post-annealed BTO:Ce films. The values have been calibrated using the lattice parameter (4.211 Å) of the MgO substrate [33]. The lattice parameters for the as-deposited films are larger than those of the BTO single crystal ($a = 3.993$, $c = 4.034$) [33], especially for sample (2) which was grown at lower oxygen pressure. The Ce doping of ~ 50 ppm will only cause about 0.01% increase in lattice parameters [27], i.e., in the magnitude of 0.0006 Å, thus the influence of Ce doping on the lattice parameters is neglected in our discussion. The larger lattice parameter normal to the substrate surface is also found in $BaTiO_3$ thin films on $SrTiO_3$ substrates fabricated by PLD [34, 37].

Table 2. Lattice parameters normal to the substrates for the as-deposited and annealed BTO:Ce thin films .

		Lattice parameters (Å)				
Sample	As-deposited	600 °C	650 °C	700 °C	750 °C	Single crystal
(1)	4.048	—	—	4.009	4.011	$a = 3.993$
(2)	4.218	—	4.073	4.067	4.046	$c = 4.034$

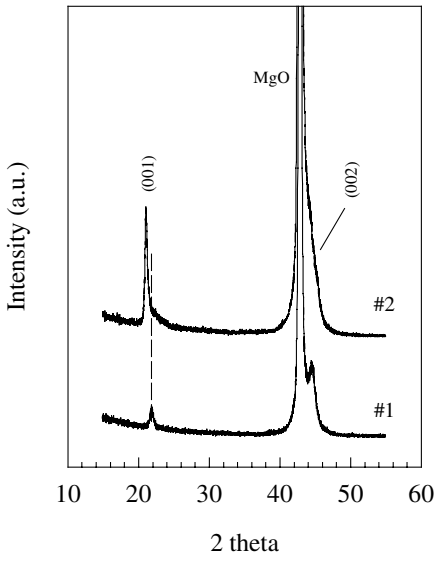

Figure 1. XRD patterns of BTO:Ce thin films deposited on MgO substrate at oxygen pressure 17 Pa (1) and 1.2×10^{-3} Pa (2), respectively. The dashed line is a guide to the eye.

The stress caused by the lattice mismatch between the substrate and the thin film affects the diffusion of the ablated particles on the substrate, and thus directly influences the lattice parameters parallel to substrate surface. It is expected that, for $BaTiO_3$ film on $SrTiO_3$ substrate, the lattice parameter parallel (normal) to substrate surface is smaller (larger) than

the corresponding one of $BaTiO_3$ single crystal due to the smaller lattice parameter of $SrTiO_3$ ($a = 3.904$ Å) and the conservation of the cell volume. However, for the thin films prepared by PLD, the oxygen pressure plays a dominant role in determining the lattice parameters [37]. It has been reported that the lattice parameters a and b parallel to the substrate surface for the c-axis oriented $BaTiO_3$ thin films on $SrTiO_3$ deposited by PLD at 3 and 7 Pa are 4.0252 and 4.0122 Å, respectively, which are larger than the a-axis lattice parameter ($a = 3.993$ Å) of $BaTiO_3$ single crystal, while the lattice parameters c are 4.0896 and 4.0162 Å, respectively. In all cases, the oxygen pressure changed from 0.1 through 3, 7, 12 to 20 Pa, the $BaTiO_3$ cell volumes are larger than that of $BaTiO_3$ single crystal, and the lower the oxygen pressure the larger the cell volume. Therefore, in our case the larger cell volumes may be expected, especially for sample (2) deposited at 1.2×10^{-3} Pa, and it is not necessary that the lattice parameters parallel to the substrate surface expand due to the larger lattice parameter of MgO substrate.

The difference in lattice parameters between the two films results from the different oxygen pressure during fabrication. When the oxygen pressure is very low, e.g., 1.2×10^{-3} Pa for sample (2), the ablated species are expected to arrive at the substrate with higher kinetic energy due to very few collisions with the oxygen species. The kinetic energy will be converted into thermal energy on impact with the substrate, causing a rise in the local temperature of the substrate and the ablated species. Therefore, the species have a larger amplitude of thermal vibrations and the resultant anharmonicity causes an increase of the mean inter-ionic distance. On the contrary, at higher oxygen pressure, e.g. 17 Pa for sample (1), the ablated species will have a larger number of collisions with the oxygen species and thus have lower kinetic energy when arriving at the substrate, resulting in smaller amplitude of thermal vibrations which in turn leads to a smaller mean inter-ionic distance [34–37].

The oxygen pressure also influences the oxygen content of BTO:Ce films [38]. It was found that lower oxygen pressure resulted in oxygen deficiency in $BaTiO_3$ films grown by the PLD technique, e.g., the ratios of Ba:Ti:O are 0.999:1:2.675 and 1.035:1:2.993, respectively, at oxygen pressures of 6 and 20 Pa. Thus, the oxygen vacancy of sample (2) deposited at 1.2×10^{-3} Pa should be significant while the oxygen vacancy of sample (1) deposited at 17 Pa is negligible. The oxygen deficiency may contribute to lattice distortion, similar to those found in $YBa_2Cu_3O_{7-\delta}$ thin films [39]. Since BTO:Ce is a highly ionic compound, the oxygen deficiency may lead to an increase in the repulsive force between cations such as Ba^+ and Ti^+, and thus causes lattice expansion.

Figure 2 shows the AFM images of the two as-deposited films, which clearly indicates that sample (2) has smaller grains and a smoother surface. The average grain size of these two films as determined from the AFM measurement is 28 nm for sample (1) and 17 nm for sample (2). It is always found that the lower the oxygen pressure, the smaller the grain size and the smoother the film surface for $BaTiO_3$ thin films grown by PLD [34, 35]. However, for $BaTiO_3$ thin films fabricated by rf-magnetron sputtering, the lower the gas pressure, the larger the grain size [36]. In general, larger species mobility promotes the growth of grains accompanied with larger surface roughness. In the case of $BaTiO_3$ thin films by PLD, the lower oxygen pressure may induce higher nuclei density resulting in smaller grain size.

The orientation of the films can be controlled by the oxygen pressure during deposition [34, 35, 37], and both as-deposited samples are preferentially c-axis oriented. After annealing at 700 °C, the lattice parameter normal to the substrate surface of sample (1) is smaller than the c-axis lattice parameter and very close to the a-axis parameter of single crystal (see table 2), indicating that the corresponding tetragonality (c/a) is smaller for this sample.

The larger lattice parameters of the as-deposited films as compared to those of crystal indicate the existence of tensile stress in the films and a larger stress for sample (2). With

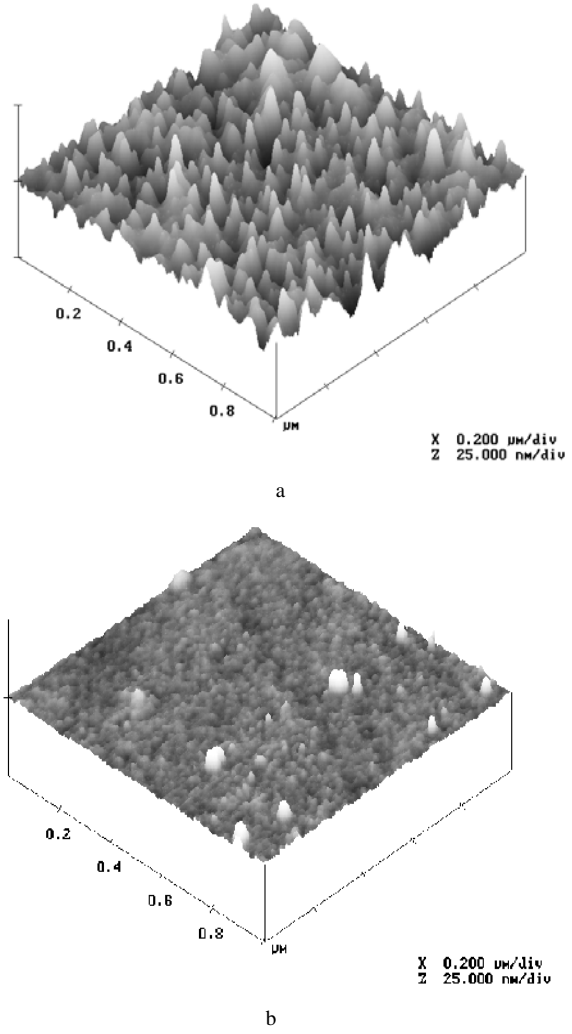

Figure 2. AFM images of the as-deposited films deposited at oxygen pressure 17 Pa (1) (a) and 1.2×10^{-3} Pa (2) (b).

increasing annealing temperature, the lattice parameters normal to the substrate surface decrease indicating the relaxation of tensile stress. At the same time, the AFM images clearly show that the grain size increases.

4. Raman results and discussion

4.1. Raman mode assignments

$BaTiO_3$ is a typical ferroelectrics with perovskite structure. Above 120 °C, it is cubic and belongs to space group $Pm3m(O_h^1)$. Between 5 and 120 °C, it is tetragonal with $P4mm(C_{4v}^1)$ symmetry [40]. In the cubic (paraelectric) phase, the 12 optic modes transform as the $3F_{1u}$ (IR) + $1F_{2u}$ irreducible representations, and there are no first-order Raman active modes. In the tetragonal (ferroelectric) phase, each F_{1u} mode splits into a A_1 mode and an E mode, while the

F_{2u} mode splits into B_1 and E, resulting in $3A_1(IR,R) + B_1(R) + 4E(IR,R)$ modes. There are further splittings (LO, TO splitting) of the vibrational modes due to long-range electrostatic forces associated with lattice ionicity. As a consequence, each A_1 or E mode splits into a pair of modes, i.e., $A_1 \rightarrow A_1(TO) + A_1(LO)$ and $E \rightarrow E(TO) + E(LO)$, where TO and LO refer, respectively, to the transverse and longitudinal optic modes [41]. We then obtain the following distinct Raman modes: $3A_1(TO) + 3A_1(LO) + 3E(TO) + 3E(LO) + 1E(LO + TO) + 1B_1$ for the room temperature tetragonal phase, $BaTiO_3$ crystals have been extensively studied by Raman spectroscopy [40–47]. The tetragonal to cubic phase transition can be easily identified by the abrupt disappearance of the sharp mode at 305 cm^{-1} which has a mixed character of the B_1 and E modes derived from the F_{2u} cubic mode [40, 41], and the disappearance of the mode at 720 cm^{-1} which is assigned to the mixture of $A_1(LO_3)$ and $E(LO_3)$ [45]. However, the two strongest Raman modes at 270 ($A_1(TO_2)$) and 510 cm^{-1} ($A_1(TO_3)$) persist into the cubic phase, which is not expected from group selection rules as the above mentioned. This has been attributed to the occurrence of the tetragonal distortion on short distance (several lattice constants) and time scales (several vibrational periods) in the cubic phase [47]. In this paper, the subscripts 1, 2 and 3 of the TO and LO modes are used merely as a method for labeling the Raman modes, where 1 refers to the lowest-frequency phonon and 3 refers to the highest-frequency phonon.

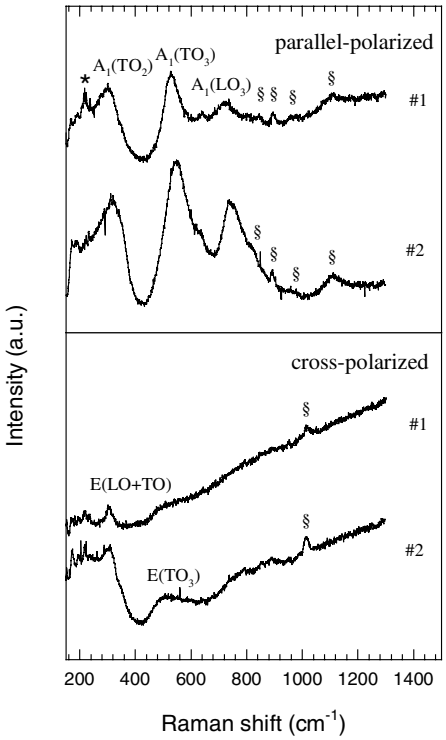

Figure 3. Parallel- and cross-polarized Raman spectra for the as-deposited BTO:Ce thin films. ⋆ corresponds to the position of the plasma line. The Raman peaks from MgO substrate are indicated by §.

4.2. Raman spectra of the as-deposited films

Figure 3 shows the parallel- and cross-polarized Raman spectra of the as-deposited BTO:Ce thin films. The polarization direction of the incident laser is along the [100] direction of the MgO substrates. Due to the notch filters used in our spectrometer and plasma lines from the

laser source, it is difficult to observe weak Raman modes below 180 cm^{-1}. The parallel-polarized peaks around 850, 895, 970 and 1110 cm^{-1}, and cross-polarized peaks at 1015 cm^{-1} are attributed to the second-order Raman peaks of the MgO substrate (indicated by § in figure 3) [48]. The weak peak at 640 cm^{-1} in the parallel-polarized geometry indicates the existence of impurity phase the anatase TiO_2 [49].

Only A_1 and B_1 modes should be observable in the parallel-polarized spectra, while only the E modes do in the cross-polarized spectra. In our backscattering geometry, only *c*-oriented domains contribute to the A_1(LO) modes while the A_1(TO) and E(TO) modes arise from *a*-domains. E(LO) modes are not observable. The assignments and frequencies of the Raman modes for the as-deposited and annealed at 700 °C BTO:Ce thin films together with those of the $BaTiO_3$ single crystal are listed in table 3. The coexistence of the A_1(LO) and A_1(TO) peaks in the parallel-polarized Raman spectra indicates that the BTO:Ce thin films contain both *a*- and *c*-domains. In general, a ferroelectric thin film is epitaxially grown in the cubic phase on single crystal MgO substrate since the substrate temperature is above its Curie temperature during deposition. Subsequent cubic to tetragonal phase transition takes place during cooling after deposition resulting in the coexistence of *a*- and *c*-domains at room temperature to relax the accumulated strain [16].

Table 3. Symmetry and frequencies of the Raman modes for the as-deposited and annealed at 700 °C BTO:Ce thin films together with those of $BaTiO_3$ single crystals.

	Single crystal			Sample (1)		Sample (2)	
Mode	Reference [40]	Reference [41]	Reference [44]	As-deposited/700 °C		as-deposited/700 °C	
$E(TO_1)$	38	38	∼ 5				
$A_1(LO_1)$	189	178	175				
$A_1(TO_1)$	178	180	165				
$E(TO_2)$	180	180					
$E(LO_1)$	180	180	180				
$A_1(TO_2)$	267	278	270	303	282	318	302
E(TO)	308	305	305	307	307	307	307
$E(LO_2)$	466	463	460				
$A_1(LO_2)$	473	470	465				
$E(TO_3)$	489	486	485	491	488	493	487
$A_1(TO_3)$	512	520	515	531	525	547	529
$E(LO_3)$	722	715	720				
$A_1(LO_3)$	740	727	720	725	725	745	728

From table 3, the frequencies of $A_1(TO_2)$ and $A_1(TO_3)$ for the as-deposited sample (1), the $A_1(TO_2)$, $A_1(TO_3)$ and $A_1(LO_3)$ modes for the as-deposited sample (2), are appreciably higher than the corresponding phonon frequencies in the $BaTiO_3$ single crystal, and sample (2) exhibits larger blue shifts.

4.3. Cause of the blue shifts of Raman modes

Both phonon confinement and stress affect Raman modes [5, 6, 25, 29, 30, 49–51]. For very small crystallites (grains), the phonons are confined in space, i.e., the breakdown of the long-range order, which causes the Raman activation of the off-centre phonons (non-zero $\boldsymbol{k}$) over the Brillouin zone, leading to the shift of the Raman modes. However, we can rule out the phonon confinement as the main cause of the blue shifts for the following reasons. (1) Using the phonon dispersion relation of the $PbTiO_3$ crystal which also has the tetragonal structure

as $BaTiO_3$ [40], the frequency of the $A_1(TO_3)$ mode should decrease whereas those of the $A_1(TO_2)$ and $A_1(LO_3)$ modes increase with $\boldsymbol{k}$ contribution, which contradict with the blue shifts of all the three Raman modes in the present case. (2) Experiments have shown that the blue shift of the $A_1(TO_3)$ mode is less than 2 cm^{-1} for grain sizes larger than 17 nm, the smallest grain size in our case [31]. Thus, we conclude that the phonon confinement effect does not play an important role in our case.

We attribute the observed blue shifts to tensile stress. For $PbTiO_3$ thin films, the Raman frequencies shift remarkably to lower frequencies compared with single crystal data and the shifts can be well accounted for by compressive stress analogous to the hydrostatic pressure effect on single crystal [6, 29, 30]. In our case of BTO:Ce thin films as well as those observed by Zhu *et al* [5, 25], the Raman modes 270 ($A_1(TO_2)$), 520 ($A_1(TO_3)$) and 720 cm^{-1} ($A_1(LO_3)$) are found at higher frequencies than the corresponding modes in single crystal. Zhu *et al* simply attributed the blue shift to the tensile stress in the films and found that the stress can be released by annealing to obtain larger grains. Here, we proceed to compare the present Raman data with the pressure effect on $BaTiO_3$ and $PbTiO_3$ crystals in order to understand the blue shift of the A_1 modes. Within the stable region of the tetragonal phase of $BaTiO_3$ below 2 GPa, the $A_1(TO_2)$ and $A_1(TO_3)$ modes shift to lower frequencies with increasing pressure, while the

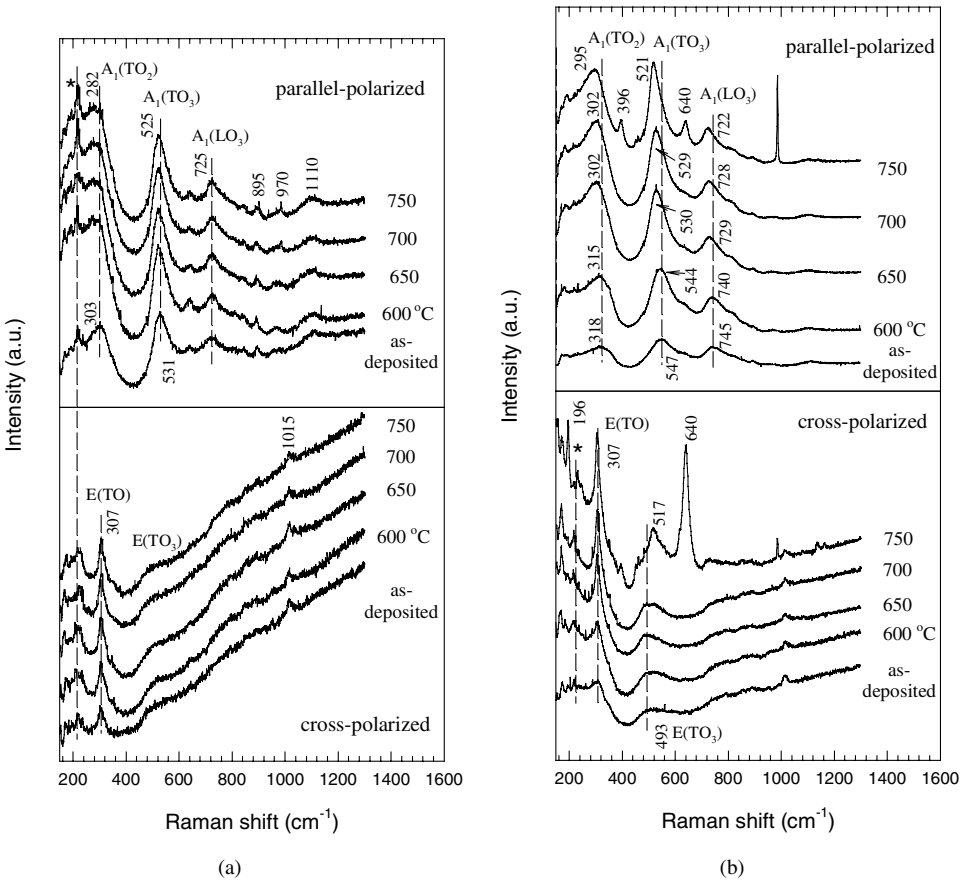

Figure 4. Polarized Raman spectra of the sample (1) (a) and (2) (b) annealed at different temperatures. The dashed lines indicated by ⋆ correspond to the positions of the plasma lines.

$A_1(LO_3)$ mode exhibits no significant shift and the sharp peak at around 305 cm^{-1} (E(LO + TO)) mode remains at the same frequency [53, 54]. The same modes of $PbTiO_3$ [55, 56] show similar pressure dependence. It is clear from the above results that the shifts of the Raman peaks for sample (1) relative to those of single crystal are opposite to the pressure effect. That is, there is an equivalent negative pressure in sample (1), i.e. tensile stress.

The Raman spectra of sample (2) also show the expected shifts due to tensile stress, i.e. the $A_1(TO_2)$ and $A_1(TO_3)$ modes move to higher frequencies, with the exception of the $A_1(LO_3)$ mode which also shows a significant blue shift. We attribute this difference in the behaviour of the $A_1(LO_3)$ mode to the large difference (0.184 Å) in the *c*-axis parameter between sample (2) and crystal, which is much larger than the *c*-axis difference (0.04 Å) between the cubic paraelectric and tetragonal ferroelectric phases where the high-pressure data are applicable.

4.4. Raman spectra after annealing

From the XRD and AFM results, annealing induces the growth of grain and the relaxation of stress. Figure 4 shows the annealing temperature dependence of the Raman spectra for the two samples and Figure 5 displays the frequency variations of $A_1(TO_2)$, $A_1(TO_3)$ and $A_1(LO_3)$ modes and linewidth variation of $A_1(TO_3)$. From figures 4 and 5, we can draw the following conclusions. (i) The Raman modes shift towards the corresponding frequencies of the $BaTiO_3$ crystals and the Raman peaks become narrower with increasing annealing temperature. No obvious spectral changes occur above 650 °C for sample (2) and above 600 °C for sample (1).

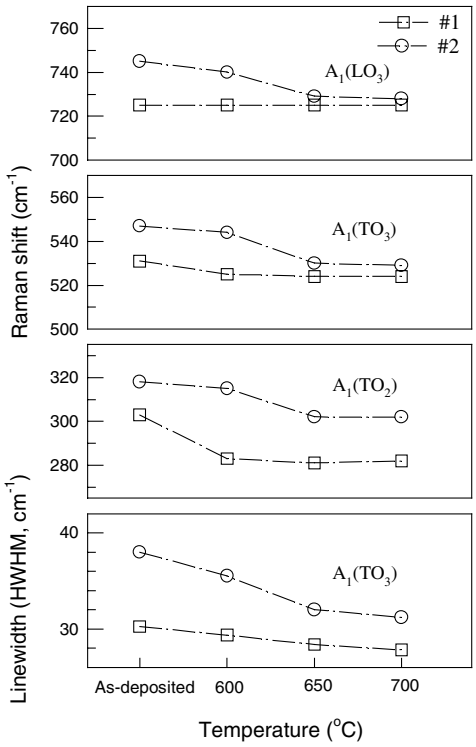

Figure 5. Annealing temperature dependence of the frequencies of the Raman modes $A_1(LO_3)$, $A_1(TO_3)$ and $A_1(TO_2)$, and linewidth of Raman mode $A_1(TO_3)$ for sample (1) and (2).

This temperature difference between the two samples is due to the larger tensile stress in sample (2). (ii) The frequency of the Raman mode at 307 cm^{-1}, which is indicative of the tetragonality (c/a) of the BTO:Ce phase, remains constant. (iii) The background at the lower frequency region increases with annealing temperature, particularly for sample (2). The background is the high-frequency tail of a mode below 100 cm^{-1}. (iv) After annealing at 750 °C, some new Raman peaks appear at 196, 396, 452, 461, 517, 640, 986, 1138 and 1163 cm^{-1} for sample (2). These peaks are indicative of the formation of the other Ba-Ti-O phases. For example, the peaks at 196, 396, 517 and 640 cm^{-1} belong to the anatase TiO_2 [48].

Besides promoting the growth of bigger grains, annealing in air may also result in more ordered arrangement of the atoms within the grains and reduce the oxygen vacancies, both of which can have a major influence on the Raman spectra. In our experiments, no significant difference was found between samples annealed in air and in vacuum in our temperature range 600–750 °C. Hence we conclude that the spectral changes observed are not caused by changes in the oxygen content.

5. Conclusions

Two thin films of Ce-doped $BaTiO_3$ grown by pulsed laser deposition on MgO (100) at different oxygen pressures have been studied using micro-Raman scattering, x-ray diffraction and atomic force microscopy. The deposition oxygen pressure has great influence on the lattice parameters, grain size and surface morphology. Films grown at lower oxygen pressure have small grains and smooth surface and the lattice parameter normal to the substrate surface are elongated. The Raman modes for the as-deposited thin films shift to higher frequencies in comparison with the frequencies of the modes in $BaTiO_3$ single crystals. It has been found that the shifts can be well accounted for by tensile stress. With increasing annealing temperature, the lattice parameters normal to the substrate surface shorten, the corresponding Raman modes shift towards those of $BaTiO_3$ single crystals and become narrower, indicating the relaxation of the tensile stress.

References

[1] Kingon A I and Myers E R (ed) 1990 *Ferroelectric Thin Films, Mater. Res. Soc. Symp. Proc. (Pittsburgh, USA)* vol 200
[2] Okuyama M and Hamakawa Y 1988 *Sensor Mater.* **1** 13
[3] Scott J F and Paz de Araujo C A 1989 *Science* **246** 1400
[4] Desu S B 1994 *Phys. Status Solidi* a **141** 119
[5] Zhu J S, Lu X M, Jiang W, Tian W, Zhu M, Zhang M S, Chen X B, Liu X and Wang Y N 1997 *J. Appl. Phys.* **81** 1392
[6] Yuzynk Y I, Farhi R, Lorman V L, Rabkin L M, Sapozhnikov L A, Sviridov E V and Zakharchenko I N 1998 *J. Appl. Phys.* **84** 452
[7] Mendiola J, Calzada M L, Ramos P, Martin M J and Agulló-Rueda F 1998 *Thin Solid Films* **315** 195
[8] Batzer R S, Yen B M, Liu D, Chen H, Kubo H and Bai G R 1996 *J. Appl. Phys.* **80** 6235
[9] Rossetti G A, Jr, Cross L E and Kushida K 1991 *Appl. Phys. Lett.* **59** 2524
[10] Pertsev N A, Zembilgotov A G and Tagantsev A K 1998 *Phys. Rev. Lett.* **80** 1988
[11] Yoneda Y, Okabe T, Sakaue K, Terauchi H, Kasatani H and Deguchi K 1998 *J. Appl. Phys.* **83** 2458
[12] Yano Y, Iijima K, Daitoh Y, Terashima T, Bando Y, Watanabe Y, Kasatani H and Terauchi H 1994 *J. Appl. Phys.* **76** 7833
[13] Fujisawa H, Shimizu M, Horiuchi T, Shiosaki T and Matsushige K 1996 *Japan. J. Appl. Phys.* **35** 4913
[14] Kwak B S, Erbi A, Budai J D, Chisholm M F, Boatner L A and Wilkens B J 1994 *Phys. Rev.* B **49** 14865
[15] Kwak B S, Erbi A, Wilkens B J, Budai J D, Chisholm M F and Boatner L A 1992 *Phys. Rev. Lett.* **68** 3733
[16] Kim S, Park Y, Park W, Baik S and Gruverman A L 1998 *Thin Solid Films* **312** 249
[17] Ren S B, Lu C J, Liu J S, Shen H M and Wang Y N 1996 *Phys. Rev.* B **54** 14337
[18] Wang C L and Smith S R P 1995 *J. Phys.: Condens. Matter.* **7** 7163

[19] Jang J W, Chung S J, Cho W J, Hahn T S and Choi S S 1997 *J. Appl. Phys.* **81** 6322
[20] Uchino K, Sadanaga E and Hirose T 1989 *J. Am. Ceram. Soc.* **72** 1555
[21] Kinoshita K and Yamaji A 1976 *J. Appl. Phys.* **47** 371
[22] Ishikawa K, Yoshikawa K and Okada N 1988 *Phys. Rev.* B **37** 5852
[23] Park Y, Cho K and Kim H G 1997 *Mater. Res. Bull.* **32** 1485
[24] Park Y and Kim Y 1996 *Mater. Res. Bull.* **31** 1479
[25] Wang B and Zhang L 1998 *Phys. Status Solidi* a **169** 57
[26] Zhu Y, Zhang D F, Dong C, Niu X J, Zhang J F and Zhou T 1997 *Ferroelectrics* **195** 69
[27] Zhu Y, Wu X and Yang G Z 1996 *Proc. SPIE* **2896** 69
[28] Liu Y W, Chen Z H, Li C L, Cui D F, Zhou Y L and Yang G Z 1997 *J. Appl. Phys.* **81** 6328
[29] Taguchi I, Pignolet A, Wang L, Proctor M, Lévy F and Schmid P E 1993 *J. Appl. Phys.* **73** 394
[30] Ching-Prado E, Reynés-Figueroa A, Katiyar R S, Majumder S B and Agrawal D C 1995 *J. Appl. Phys.* **78** 1920
[31] Begg B D, Finnie K S and Vance E R 1996 *J. Am. Ceram. Soc.* **79** 2666
[32] Cui D F, Li C L, Ma K, Zhou Y L, Liu Y W, Chen Z H, Ma J W and Li L 1996 *Appl. Phys. Lett.* **68** 750
[33] Yoneda Y, Okabe T, Sakaue K, Terauchi H 1998 *Surf. Sci.* **410** 62
[34] Zhang J, Cui D F, Zhou Y L, Li L, Chen Z H, Szabadi M and Hess P 1996 *Thin Solid Films* **287** 101
[35] Nakata Y, Soumagne G, Okada T and Maeda M 1998 *Appl. Surf. Sci.* **127–129** 650
[36] Lee N Y, Sekine T, Ito Y and Chino K U 1994 *Japan. J. Appl. Phys.* **33** 1484
[37] Li C L, Cui D F, Zhou Y L, Lu H B, Chen Z H, Zhang D F and Wu F 1998 *Appl. Surf. Sci.* **136** 173
[38] Li W, Lu F, Liu Z G, Zhu Y, Wang F X, Liu X D, Tan C Y and Wang K M 1999 *Thin Solid Films* **340** 68
[39] Jorgensen J D, Veal B W, Paulikas A P, Nowicki L J, Crabtree G W, Claus H and Kwok W K 1990 *Phys. Rev.* B **41** 1863
[40] Freire J D and Katiyar R S 1988 *Phys. Rev.* B **37** 2074
[41] DiDomenico M Jr, Wemple S H and Porto S P S 1968 *Phys. Rev.* **174** 522
[42] Loudon R 1964 *Adv. Phys.* **13** 423
[43] Rimai L, Parsons J L, Hickmott J T and Nakamura T 1968 *Phys. Rev. 168* 623
[44] Pinczuk A, Taylor W and Burstein E 1967 *Solid State Commun.* **5** 429
[45] Parsons J L and Rimai L 1967 *Solid State Commun.* **5** 423
[46] Chaves A, Katiyar R S and Porto S P S 1974 *Phys. Rev.* B **10** 3522
[47] Sanjurjo J A, Katiyar R S and Porto S P S 1980 *Phys. Rev.* B **22** 2396
[48] Robins L H, Kaiser D L, Rotter L D, Schenck P K, Stauf G T and Rytz D 1994 *J. Appl. Phys.* **76** 7487
[49] Zhang Y H, Chan C K, Porter J F and Guo W 1998 *J. Mater. Res.* **13** 2602
[50] Richter H, Wang Z P and Ley L 1981 *Solid State Commun.* **39** 625
[51] dos Santos D R and Torriani I L 1993 *Solid State Commun.* **85** 307
[52] Bersani D, Lottici P P and Ding X Z 1998 *Appl. Phys. Lett.* **72** 73
[53] Sood A K, Chandrabhas N, Muthu D V S and Jayaraman A 1995 *Phys. Rev.* B **51** 8892
[54] Venkateswaran U D, Naik V M and Naik R 1998 *Phys. Rev.* B **58** 14256
[55] Cerdeira F, Holzapfel W B and Bäuerle D 1975 *Phys. Rev.* B **11** 1188
[56] Sanjurjo J A, López-Cruz E and Burns G 1983 *Phys. Rev.* B **28** 7260